machines

Article

A Velocity-Adaptive MPC-Based Path Tracking Method for Heavy-Duty Forklift AGVs

Yajun Wang [1], Kezheng Sun [2,3], Wei Zhang [2,*] and Xiaojun Jin [3]

1 State Energy Group Shendong Coal Group Co., Ltd., Yulin 719315, China; yajun.wang.h@chnenergy.com.cn
2 College of Mechanical and Electronic Engineering, Nanjing Forestry University, Nanjing 210037, China; sunkznjfu@163.com
3 Zhongcang Robot (Nanjing) Co., Ltd., Nanjing 211899, China; xiaojun.jin@outlook.com
* Correspondence: zhangwnjfu@163.com

Abstract: In warehouses with vast quantities of heavy goods, heavy-duty forklift Automated Guided Vehicles (AGVs) play a key role in facilitating efficient warehouse automation. Due to their large load capacity and high inertia, heavy-duty forklift AGVs struggle to automatically navigate optimized routes. Additionally, rapid acceleration and deceleration can pose safety hazards. This paper proposes a velocity-adaptive model predictive control (MPC)-based path tracking method for heavy-duty forklift AGVs. The movement of heavy-duty forklift-type AGVs is categorized into straight-line and curve-turning motions, corresponding to the straight and curved sections of the reference path, respectively. These sections are segmented based on their curvature. The best driving speeds for straight and curved sections were 1.5 m/s and 0.3 m/s, respectively, while the optimal acceleration rates were 0.2 m/s^2 for acceleration and -0.2 m/s^2 for deceleration in straight paths and 0.3 m/s^2 for acceleration with -0.15 m/s^2 for deceleration in curves. Moreover, preferred sampling times, prediction domain, and control domain were determined through simulations at various speeds. Four path tracking methods, including pure tracking, Linear Quadratic Regulator (LQR), MPC, and the velocity-adaptive MPC, were simulated and evaluated under straight-line, turning, and complex double lane change conditions. Field experiments conducted in a warehouse environment demonstrated the effectiveness of the proposed path tracking method. Findings have implications for advancing path tracking control in narrow aisles.

Keywords: heavy-duty forklift AGV; path tracking; MPC; velocity-adaptive control

check for updates

Citation: Wang, Y.; Sun, K.; Zhang, W.; Jin, X. A Velocity-Adaptive MPC-Based Path Tracking Method for Heavy-Duty Forklift AGVs. *Machines* **2024**, *12*, 558. https://doi.org/10.3390/machines12080558

Academic Editor: Raffaele Di Gregorio

Received: 14 July 2024
Revised: 12 August 2024
Accepted: 14 August 2024
Published: 15 August 2024

1. Introduction

In recent years, the rapid advancements in technology and the forces of economic globalization have gradually diminished the competitiveness of traditional industrial production and transportation methods [1]. AGV is a type of mobile robot that generally consists of a mechanical structure, power unit, control system, human–machine interaction system, etc. They can travel along predefined paths assigned by scheduling systems, autonomously avoid obstacles in the path, and facilitate the automated transportation of materials. These capabilities greatly improve production efficiency and industrial competitiveness [2]. Currently, AGVs have been widely used in many industries such as military [3], aviation [4], warehousing and logistics [5], manufacturing [6], agriculture and forestry [7], household services [8], and food industries [9]. As demand for intelligent and unmanned logistics management grows, industries involved in heavy-duty goods storage, including railways and ports, are increasingly compelled to enhance their intelligent systems [10]. The development of intelligent heavy-duty AGV forklifts has become critical for ensuring efficient goods handling and warehouse management [11]. However, heavy-duty AGV forklifts are typically large and become substantially heavier when loaded with goods. In such scenarios, the challenges associated with high inertia and the difficulty in initiating and halting movement become more pronounced. These challenges can lead to deviations from intended paths, instability, or even accidents such as tipping or dropping goods, particularly when acceleration changes abruptly. Traditional smooth path planning methods, which work well for smaller AGVs, often fall short under these conditions due to their inability to adequately account for the dynamics of heavy loads and the need for more sophisticated control strategies that can manage the increased inertia and complexity of movement. Therefore, it is essential to develop path tracking algorithms that are suitable for heavy-duty forklift AGVs.

Previous researchers have invested great effort in tracking paths for AGVs using proportional-integral-derivative control [12] or state feedback control [13]. However, these methods often lack robustness in situations involving uncertainties and disturbances. Recently, MPC algorithms [14] have been extensively applied in path tracking. MPC is highly robust and easy to implement. It predicts future states and control inputs over a certain time horizon and then calculates the optimal control input for the current moment based on these predictions. To optimize the path tracking ability of AGVs in complex warehouse environments, researchers have introduced the kinematic properties of vehicles into MPC algorithms. Hu et al. [15] developed an MPC algorithm based on the kinematic model of a tractor with a maximum travel speed of 1 m/s. Through adaptive time-domain adjustments, the lateral control deviation for straight and curved segments was less than 0.07 m and 0.15 m, respectively. Wang et al. [16] developed an MPC algorithm with control constraints based on the kinematics model of Mecanum wheel AGVs, which can effectively improve the tracking accuracy. Barreno et al. [17] designed an MPC algorithm for AUVs that can resist disturbances from underwater environments. The algorithm was characterized by low computational costs and high stability under various disturbance conditions. These studies have demonstrated that incorporating the vehicle kinematic model enhances the MPC algorithm's performance. However, there is limited research on the path tracking of heavy-duty forklift AGVs. The MPC algorithms based on kinematic models developed for regular AGVs may not satisfy the specific operational demands of heavy-duty forklift AGVs, thereby necessitating further research.

Heavy-duty forklift AGVs carry larger loads compared to regular ones. If the AGV accelerates too quickly or stops abruptly while driving, the sudden change in acceleration may cause the materials to slide due to their inertia, resulting in pallets sliding off the forks. In this case, the materials may fall and damage goods, posing risks to the safety of surrounding personnel. Additionally, the AGV itself could lose control [18]. Heavy-duty forklift-style AGVs are often equipped with larger counterweights. High-speed turns can cause materials to shift toward the pallet's outer edge, disrupting balance and potentially tipping the pallet. This instability could eventually lead to the AGV overturning. In practical operations, inappropriate speed settings may prevent a heavy-duty forklift-style AGV from adjusting its front wheel angle in time, causing the vehicle to deviate from the reference path and collide with shelves or walls [19]. Furthermore, in warehouses with numerous narrow aisles, significant lateral error while traveling along the reference path may lead to collisions with shelves. This requires higher control precision. For heavy-duty forklift AGVs, the path tracking algorithm should feature three key characteristics: (1) Enhancing control precision and minimizing lateral error; (2) Tailoring target speeds for straight and curved segments to ensure safe maneuvering; (3) Facilitating smooth acceleration and deceleration.

To address the path tracking challenges for heavy-duty forklift-style AGVs, this paper proposed a velocity-adaptive MPC (VA-MPC) algorithm to achieve smooth speed transitions on reference paths with different curvatures. The main contributions of this research were as follows:

(1) A velocity-adaptive MPC algorithm was proposed to address the challenges faced by heavy-duty forklift-style AGVs in warehouse environments.

(2) The movement of heavy-duty forklift-style AGVs was categorized into straight-line and curve-turning motions, with the reference path divided into corresponding straight and curved sections based on curvature.
(3) The optimal sampling times, prediction horizon, and control horizon for low-speed driving were determined through simulation analysis.
(4) Field experiments were carried out in a warehouse environment using a heavy-duty forklift AGV to validate the feasibility and effectiveness of the proposed method.

2. Materials and Methods

2.1. Overview

The overarching methodology of this research was structured to systematically address the challenges associated with the path tracking of heavy-duty forklift AGVs. It considered the unique physical characteristics and operational constraints of heavy-duty forklifts, such as large inertia and the complexities of handling heavy loads in narrow aisles. Firstly, a kinematic model for heavy-duty forklift AGVs was established. Building upon this kinematic model, we proposed a velocity-adaptive MPC algorithm to enhance control accuracy, reduce lateral errors, and achieve smooth speed transitions during start-up and stopping. Subsequently, a path partitioning method based on path curvature was developed to optimize the operation speed of heavy-duty forklift AGVs under varying path curvatures. Simulations were conducted using MATLAB (R2022a) to verify the algorithm's reliability, complemented by field experiments in a warehouse environment to assess the practical application and robustness of the developed methods under real-world conditions.

2.2. Prediction Model

The heavy-duty forklift-style AGV used in this paper has a three-wheel, single-axle structure, with driving power and steering control provided by the front steering wheel. There is a pair of auxiliary wheels under the rear fork teeth, which do not provide power and cannot steer, serving solely as balance support. This three-wheel structure is simple, provides good traction, and is widely used in intelligent warehouse handling.

The kinematic model typically employs the bicycle model, which needs to satisfy the following assumptions:

(1) The body and suspension systems are considered rigid, with no deformation.
(2) The AGV's motion is constrained to a two-dimensional plane with no vertical movement.
(3) The auxiliary wheels on the left and right fork teeth always maintain the same steering angle and displacement.
(4) There is no relative sliding between the wheels and their contact points on the ground.
(5) The AGV operates at a low speed.
(6) Air resistance is neglected.

The heavy-duty forklift-style AGV used in this study is a rigid system designed for flat warehouse environments, with a maximum speed of only 1.5 m/s. These conditions align well with the assumptions listed above. Therefore, the kinematic model was simplified to the bicycle model, as shown in Figure 1, where the motion of the two auxiliary wheels was combined into the motion of one wheel, located at the red dot M at the center of the line connecting the two auxiliary wheels.

Based on Figure 1, the kinematic equations of the forklift AGV can be obtained:

$$\begin{bmatrix} \dot{x} \\ \dot{y} \\ \dot{\varphi} \\ \dot{v} \end{bmatrix} = \begin{bmatrix} v\cos\ \varphi \\ v\sin\ \varphi \\ v\tan\ \delta/L_d \\ a \end{bmatrix} = \begin{bmatrix} f_1 \\ f_2 \\ f_3 \\ f_4 \end{bmatrix} \tag{1}$$

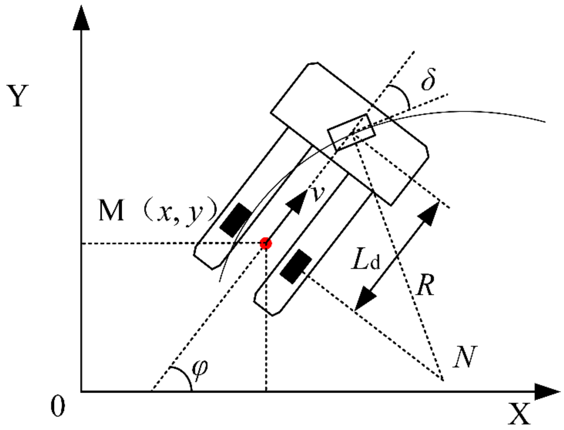

Figure 1. Simplified kinematic model.

Selecting the state variable as $\boldsymbol{\chi} = [x,\ y, \varphi, v]^T$, where x and y represent the coordinates of the vehicle's position, φ denotes the heading angle, and v is the velocity of the vehicle. The control variable $\boldsymbol{u} = [a,\ \delta]^T$ consists of acceleration a and the steering angle δ. For any reference point in the reference path denoted by r, the equation can be rewritten as follows:

$$\dot{\boldsymbol{\chi}}_r = f(\boldsymbol{\chi_r}, \boldsymbol{u_r}) \tag{2}$$

Constructing the linear state-space representation of the forklift AGV kinematic model, where $\widetilde{\boldsymbol{\chi}}(k)$ and $\widetilde{\boldsymbol{u}}(k)$ represent the changes in the error of the state variables and the control variables, respectively. Expanding the above equation at the reference point using a Taylor series and neglecting terms of order higher than quadratic, we obtain

$$\widetilde{\boldsymbol{\chi}}(k+1) = (TA+E)\widetilde{\boldsymbol{\chi}}(k) + TB\widetilde{\boldsymbol{u}}(k) = \widetilde{A}\widetilde{\boldsymbol{\chi}}(k) + \widetilde{B}\widetilde{\boldsymbol{u}}(k) \tag{3}$$

where

$$\widetilde{A} = \begin{bmatrix} 1 & 0 & -Tv_r\sin\ \varphi_r & T\cos\ \varphi_r \\ 0 & 1 & Tv_r\cos\varphi_r & T\sin\ \varphi_r \\ 0 & 0 & 1 & T\tan\ \varphi_r/L_d \\ 0 & 0 & 0 & 1 \end{bmatrix}, \widetilde{B} = \begin{bmatrix} 0 & 0 \\ 0 & 0 \\ 0 & Tv_r/L_d\cos^2\delta_r \\ T & 0 \end{bmatrix}$$

$\widetilde{A}$ and $\widetilde{B}$ represent the state matrix and control matrix, respectively. The above equation represents the discrete state-space equation of the forklift AGV kinematic model, completing the linearization of the nonlinear motion model system. Here, T represents the sampling time, the state variable is the difference between the current actual coordinates of the forklift AGV and the reference pose, and the control variable consists of velocity and front wheel angle.

Defining the prediction horizon as N_P and the control horizon as N_C, and given that $1 \leq N_\mathrm{C} \leq N_\mathrm{P}$, then the output equation can be defined as follows:

$$\boldsymbol{Y} = \boldsymbol{\psi}\xi(k) + \boldsymbol{\Theta}\Delta U \tag{4}$$

where Y represents the prediction error vector; Ψ represents the system state transition matrix; ΔU represents the control increment vector; and Θ represents the system response matrix, describing the influence of control increments on the prediction error.

2.3. Objective Function

To facilitate subsequent optimization, the solution of the model predictive control was converted into a quadratic programming problem. First, the reference value of the system output variables was defined as follows:

$$\boldsymbol{Y}_r = \left[\eta_r(k+1)\ \ \eta_r(k+2)\ \ \ldots\ \ \eta_r(k+N_c)\ \ \ldots\ \ \eta_r\left(k+N_p\right)\right]^T \tag{5}$$

Let $\boldsymbol{E} = \boldsymbol{\psi}\xi(k)$, $\boldsymbol{Q}_Q = \boldsymbol{I}_{N_p} \otimes \boldsymbol{Q}$, $\boldsymbol{R}_R = \boldsymbol{I}_{N_p} \otimes \boldsymbol{R}$, where $\otimes$ represents the Kronecker product. According to optimal control theory, the optimization objective function was defined as follows:

$$\min_{\Delta U} J = 2\left(\frac{1}{2}\Delta\boldsymbol{U}^T\boldsymbol{H}\Delta\boldsymbol{U} + \boldsymbol{g}^T\Delta U\right) \Longleftrightarrow \min_{\Delta U} J = \frac{1}{2}\Delta\boldsymbol{U}^T\boldsymbol{H}\Delta\boldsymbol{U} + \boldsymbol{g}^T\Delta U \tag{6}$$

2.4. Constraint Conditions

In the path tracking algorithm presented in this paper, the primary control focused on the magnitude and rate of change of the speed and front wheel angle of the heavy-duty forklift-style AGV. By recursive control, the following equations for control variables and control increments can be obtained:

$$\begin{aligned}
\widetilde{\boldsymbol{u}}(k) &= \widetilde{\boldsymbol{u}}(k-1) + \Delta\widetilde{\boldsymbol{u}}(k) \\
\widetilde{\boldsymbol{u}}(k+1) &= \widetilde{\boldsymbol{u}}(k) + \Delta\widetilde{\boldsymbol{u}}(k+1) = \widetilde{\boldsymbol{u}}(k-1) + \Delta\widetilde{\boldsymbol{u}}(k) + \Delta\widetilde{\boldsymbol{u}}(k+1) \\
&\ \ \vdots \\
\widetilde{\boldsymbol{u}}(k+N_C-1) &= \widetilde{\boldsymbol{u}}(k+N_C-2) + \Delta\widetilde{\boldsymbol{u}}(k+N_C-1) = \widetilde{\boldsymbol{u}}(k-1) + \ldots\Delta\widetilde{\boldsymbol{u}}(k+N_C-1)
\end{aligned} \tag{7}$$

By adding maximum and minimum constraints to the control variables, the model predictive control problem was transformed into a standard quadratic programming problem, as shown in Equation (8):

$$\begin{aligned}
&\min_{\Delta U} J = \tfrac{1}{2}\Delta\boldsymbol{U}^T\boldsymbol{H}\Delta\boldsymbol{U} + \boldsymbol{g}^T\Delta\boldsymbol{U} \\
&s.t.\begin{cases} \boldsymbol{U}_{min} \le \boldsymbol{U}_t + \boldsymbol{D}_I\Delta U \le \boldsymbol{U}_{max} \\ \Delta\boldsymbol{U}_{min} \le_I \Delta U \le \Delta\boldsymbol{U}_{max} \end{cases}
\end{aligned} \tag{8}$$

2.5. Velocity-Adaptive MPC Algorithm Based on Path Curvature

2.5.1. Velocity-Adaptive Strategy

Setting different operating speeds for straight and curved segments can effectively prevent cargo slippage and ensure smooth operation of the heavy-duty forklift AGV. In this study, the heavy-duty forklift-style AGV can accelerate to 1.5 m/s on straight segments while maintaining stability. However, during curved turns, the vehicle was at risk of veering off the path or colliding with walls. To ensure operational safety, the entire path was divided into straight and curved segments based on their curvatures. In each segment, the heavy-duty forklift-style AGV undergoes a process of starting, accelerating, decelerating, and stopping. Due to constraints imposed by the physical environment, the operating speed of the heavy-duty forklift-style AGV varies across different segments. Therefore, the core of velocity-adaptive control lies in designing different speeds and accelerations for segments with different curvatures.

2.5.2. Optimal Time Domain Solution

The prediction horizon N_P and control horizon N_C are crucial parameters affecting control accuracy and stability. Selecting appropriate prediction and control horizons can significantly enhance path tracking quality [20]. As depicted in Figure 2a, a larger prediction horizon enabled the controller to predict motion states over a longer distance. However, larger tracking errors nearby may accumulate over time, leading to gradually increasing deviations. In contrast, a shorter prediction horizon offers advantages in real-time tracking but reduces the prediction length. Under constraints on the control increment of the front wheel steering angle, as illustrated in Figure 2b, the forklift AGV may fail to steer promptly.

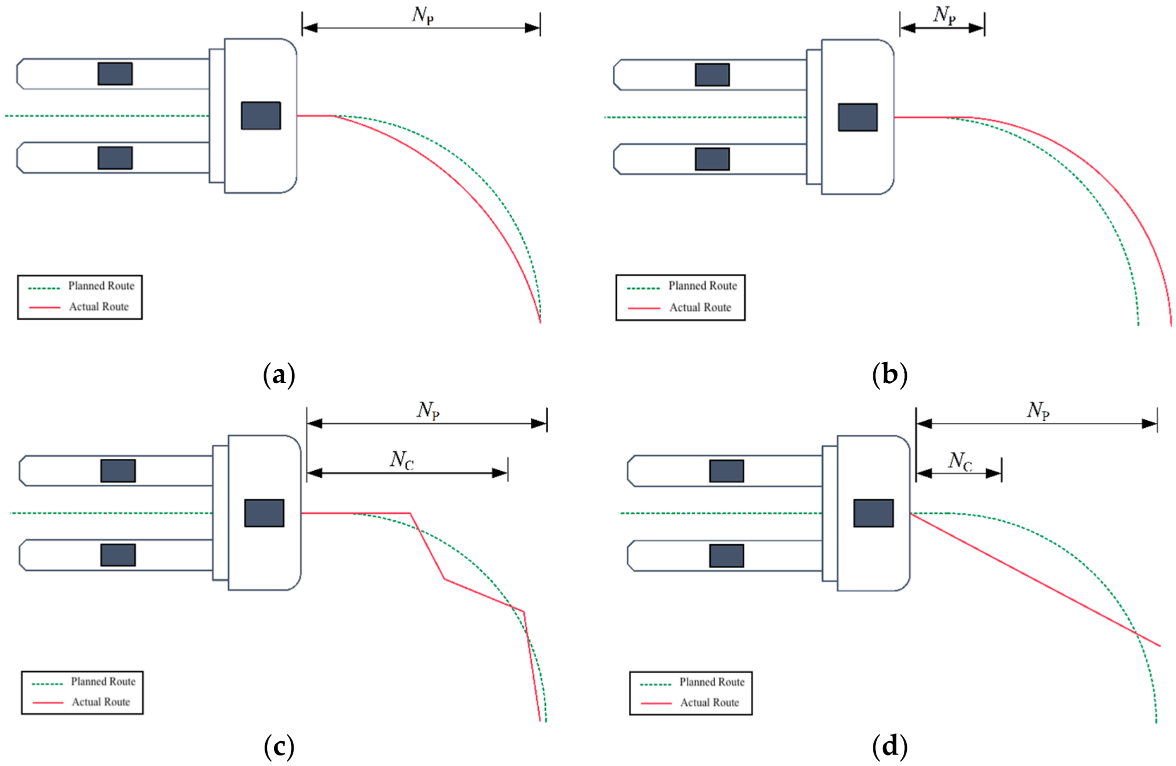

Figure 2. Effect of N_C and N_P on tracking performance: (**a**) Impact of oversized N_P; (**b**) Impact of undersized N_P; (**c**) Impact of oversized N_C; (**d**) Impact of undersized N_C.

When the prediction horizon remains constant but the control horizon increases, the system exhibits better real-time control. However, an overly sensitive controller can lead to a decrease in control accuracy, as depicted in Figure 2c. Conversely, Figure 2d shows that a smaller control horizon enhanced system stability but at the cost of significantly reduced control accuracy and increased tracking errors. Therefore, it is necessary to determine different prediction and control horizons for varying speeds to achieve an optimal balance between system stability and tracking accuracy.

The maximum max(e_y), minimum min(e_y), and mean avg(e_y) values of lateral error indicate the extreme tracking performance, while the standard deviation σ(e_y) of the lateral error indicates the stability of the path tracking. Since the minimum value is extremely small, it is not considered the primary criterion for evaluation. An evaluation function, as shown in Equation (9), incorporates the maximum, mean, and standard deviation of lateral error.

$$C_e = 0.2\max\left(e_y\right) + 50avg\left(e_y\right) + 3\sigma\left(e_y\right) \tag{9}$$

2.6. Heavy-Duty Forklift AGV Path Tracking Experiment

To validate the feasibility and effectiveness of the velocity-adaptive MPC-based path tracking method for heavy-duty forklift AGVs, field experiments were carried out in a warehouse environment (Figure 3) using a heavy-duty forklift AGV developed by Zhongcang Robot (Nanjing) Co., Ltd. (Figure 4).

Figure 3. Warehouse environment for path tracking experiment.

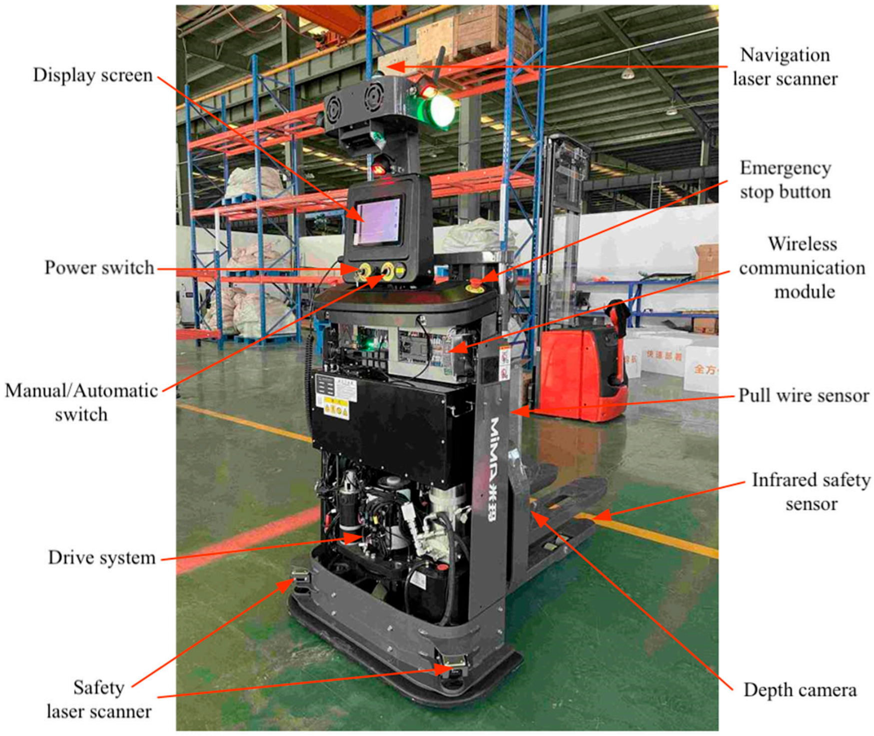

Figure 4. The main components of the heavy-duty forklift AGV.

2.6.1. Heavy-Duty Forklift AGV System

The navigation module of the heavy-duty forklift AGV utilized real-time feedback from the navigation laser scanner to accurately determine the vehicle's position. The motion detection module collected and processed parameters such as vehicle speed and steering angles. The vision module, connected to a depth camera, facilitated precise short-range image recognition. The control system of the heavy-duty forklift AGV interpreted the motion status data to manage the actions of the drive motor and steering motor, ensuring smooth operation within the warehouse. The safety module is a critical component of the heavy-duty forklift AGVs. Safety laser sensors on both sides of the vehicle front and infrared safety sensors at the fork ends detected obstacles close to the ground. A laser scanner mounted on the top of the vehicle scanned for obstacles at higher elevations to prevent collisions with high-level racks. Figure 4 illustrates the heavy-duty forklift AGV and its main components, while the parameters of the heavy-duty forklift AGV are presented in Table 1.

Table 1. Parameters of the heavy-duty forklift AGV.

Parameter Name	Value	Unit
Lifting height	1600	mm
Dimensions (L/W/H)	1714/1025/1937	Length/Width/Height (mm)
Wheelbase	0.88	m

The control system of the heavy-duty forklift AGV was developed based on the Robot Operating System (ROS) platform (Linux Ubuntu 16.0). The warehouse management system selected a forklift AGV for loading and unloading tasks and planned a feasible reference path from the AGV's starting point to the designated location. This reference path, along with the task, was then transmitted to the forklift AGV, which followed the path for motion tracking control. During the tracking process, the AGV's laser and infrared sensors continuously scanned the surrounding environment, providing feedback to the controller to allow real-time adjustments. The ROS system's modular programming and message-passing mechanisms effectively integrated the vehicle's sensors with the onboard and higher-level systems. This integration enabled the forklift AGV to perform real-time monitoring during motion control, thereby enhancing operational safety.

2.6.2. Experiment Design

The experiment was designed to include a comprehensive path consisting of straight sections, curved sections, and loading/unloading segments. Considering the obstacles in the experimental site, Node 31 (pallet) was set as the target node, and Node 35 (coordinates (−3.6, −12.4)) was set as the starting node in Figure 5a. The initial heading angle was $\pi/2$, and the path direction was indicated by the blue arrows. Figure 5b shows the complete experimental reference path planned after selecting the nodes.

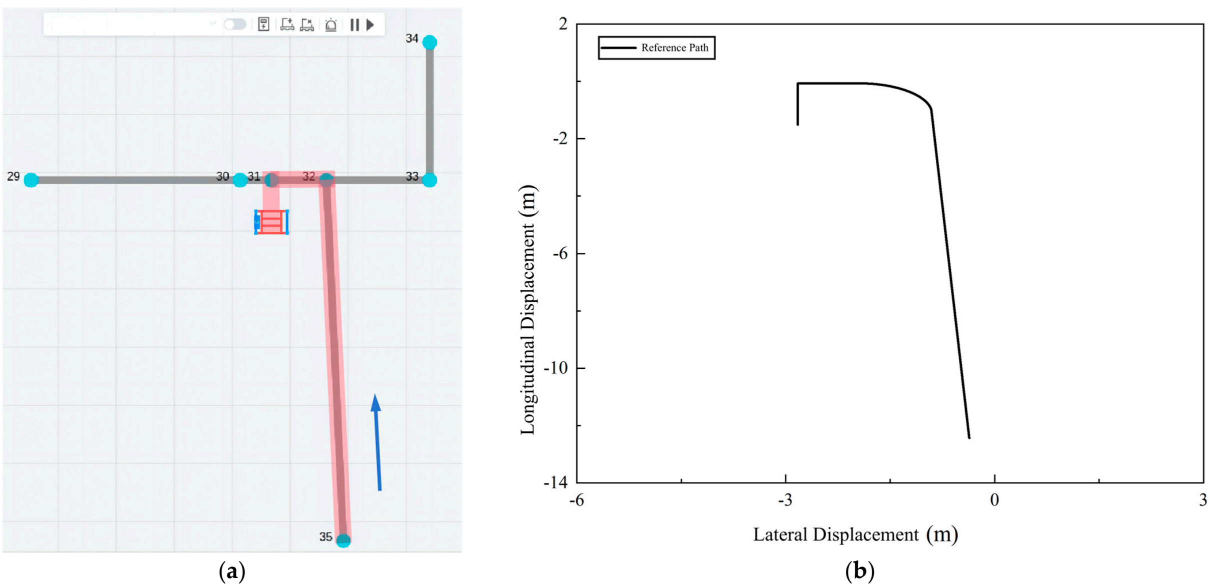

Figure 5. Experimental paths: (**a**) Schematic path in the scheduling system; (**b**) Reference path.

To prevent the heavy-duty forklift AGV from being affected by other environmental factors or hardware/software limitations during actual operation, the maximum allowable lateral deviation within the safety distance was set to 0.1 m. Thus, the lateral deviation safety threshold for real-time path tracking was 0.1 m.

3. Results

3.1. Speed and Acceleration in Different Path Segments

After conducting safety tests, the maximum speeds for straight and curved segments were set at 1.5 m/s and 0.3 m/s, respectively. In this study, the model predictive control algorithm for the heavy-duty forklift AGV utilized acceleration as the control variable to regulate the rate of speed changes, thus achieving smooth speed transitions. For straight segments, the accelerations during the acceleration and deceleration phases for the heavy-duty forklift AGV were set at 0.2 m/s^2 and $-$0.2 m/s^2, respectively. For curved segments, the accelerations during the acceleration and deceleration phases were set at 0.3 m/s^2 and $-$0.15 m/s^2, respectively.

3.2. Optimal Time Domain Values for Path Tracking

The tracking performance of the system under different prediction horizons and control horizons was tested [20,21]. The sampling periods, with N_P = 60 and N_C = 30, were more suitable for low-speed driving, and the sampling times were set to 0.1 s, 0.15 s, and 0.2 s, respectively.

The simulation results for the three different sampling times are shown in Table 2. Sampling times of 0.3 s and 1.5 s were applied to all curved and straight segments. The sampling time yielding the lowest evaluation value was selected for each speed. As shown in Table 2, the optimal sampling time for a speed of 0.3 m/s (curved segments) was 0.15 s. This resulted in the minimum average lateral error and a small standard deviation, indicating high control stability. For straight segments, a sampling time of 0.1 s resulted in the lowest maximum, average, and standard deviation of lateral tracking errors, with evaluation values significantly lower than the other two datasets, indicating optimal system performance.

Table 2. Tracking effect for three sampling times.

Speed/(m/s)	Sampling Time/s	max(e_y)/m	avg(e_y)/m	σ(e_y)/m	Ce
0.3	0.1	0.5008	0.0058	0.0381	0.5068
0.3	0.15	0.5013	0.0056	0.0400	0.5001
0.3	0.2	0.5018	0.0058	0.0406	0.5105
1.5	0.1	0.5028	0.0059	0.0398	0.5146
1.5	0.15	0.5043	0.0070	0.0423	0.5800
1.5	0.2	0.5058	0.0074	0.0439	0.6041

After obtaining the optimal sampling time, it is necessary to determine N_P and N_C to minimize tracking errors and ensure high stability for both straight and curved path segments. Kanchwala [22] reported that the MPC controller achieved superior performance when $2N_C < N_P < 3N_C$. Moreover, the system tracking performance was demonstrated to be optimal when N_P = 60 and N_C = 30 for both 0.3 m/s and 1.5 m/s running speeds [21]. In this study, different values of N_P and N_C were gathered (Table 3) to carry out simulation analysis.

Table 3 presents the dual-time-domain test results for driving speeds of 0.3 m/s and 1.5 m/s. For a speed of 0.3 m/s, results indicated that when N_P = 40, N_C = 20, and N_P = 60, N_C = 20, the evaluation function consistently reached its minimum value of 0.5098560601. Additionally, the maximum, average, and standard deviation of lateral tracking errors under both time domains were identical, indicating consistent algorithm performance. In the practical motion of the forklift AGV, smaller prediction and control horizons reduce the computational load on the controller, thereby improving system responsiveness. Therefore, prediction and control horizons were set to N_P = 40 and N_C = 20 for a running speed of 0.3 m/s. The dual-time-domain test results for the target speed of 1.5 m/s are also presented in Table 3. The minimum value of the evaluation function was 0.5125959351 when N_P = 30 and N_C = 10. Compared with the results of other time domain groups, when N_P = 30 and N_C = 10, the maximum, average, and standard deviation of lateral tracking errors were also the lowest, indicating high tracking accuracy and controller stability. As a result, the prediction and control horizons for the target speed of 1.5 m/s were set to 30 and 10, respectively.

Table 3. Time domain test results for different speeds.

Speed/(m/s)	N_P	N_C	max(e_y)/m	avg(e_y)/m	σ(e_y)/m	Ce
0.3	20	10	0.5018036863	0.0059773850	0.0409266374	0.5220099005
	30	10	0.5018035290	0.0057747638	0.0405801284	0.5108392799
	40	20	0.5018035030	0.0057564466	0.0405576758	0.5098560601
	50	20	0.5018035103	0.0057630749	0.0405702908	0.5102253210
	60	20	0.5018035030	0.0057564466	0.0405576758	0.5098560601
	60	30	0.5018035153	0.0057675605	0.0405788213	0.5104751909
1.5	20	10	0.5027995271	0.0059171427	0.0398204626	0.5158784293
	30	10	0.5027994985	0.0058569191	0.0397300265	0.5125959351
	40	20	0.5027995197	0.0058918055	0.0397827324	0.5144983766
	50	20	0.5027995188	0.0058896304	0.0397795041	0.5143799358
	60	20	0.5027995177	0.0058870502	0.0397756667	0.5142394111
	60	30	0.5027995202	0.0058928766	0.0397843060	0.5145566505

In general, when the forklift AGV travels and transports goods in a large warehouse, it spends the most time at the highest operating speed on each segment of the path. To reduce the complexity of system calculations, the optimal prediction horizon and control horizon corresponding to the fastest speed were directly applied as the time-domain parameters for each straight or curved segment. All time-domain parameters determined for straight segments and curved segments, including sampling time (t), maximum speed (v_{max}), acceleration phase acceleration (a_+), deceleration phase acceleration (a_-), prediction horizon (N_P), and control horizon (N_C) are presented in Table 4.

Table 4. Parameters of different road sections.

Path	t/s	vmax/(m/s)	a_+/(m/s^2)	A_-/(m/s^2)	N_P	N_C
Curve	0.15	0.3	0.3	−0.15	40	20
Straight	0.1	1.5	0.2	−0.2	30	10

3.3. Simulation Verification of Path Tracking

Three types of working conditions, including straight-line, turning, and double lane change conditions, were designed using the MATLAB (R2022a) simulation environment. Conventional straight-line and turning conditions were used to verify the accuracy of the tracking algorithm, while double lane change condition was used to verify the tracking stability of the algorithm under complex conditions. Both the typical path tracking algorithm (PP, LQR, MPC) and the improved path tracking algorithm were simulated separately, and their tracking effects were compared. During comparison, the preview distance of the pure tracking algorithm was set to the path length required for acceleration in the improved algorithm.

3.3.1. Straight-Line Condition

First, the straight-line condition of the heavy-duty forklift AGV was simulated and verified, representing the most common scenario in actual operation. As shown in Figure 6a, the straight segment started at position (0, 0) with an initial heading angle of 0 and an initial velocity of 0.1 m/s. As illustrated in Figure 6b, the LQR algorithm initially tracked the reference path, while the pure tracking algorithm lagged, exhibiting significant path oscillation. Both the improved algorithm and the original MPC algorithm exhibited a consistent overall tracking trend, with the improved algorithm slightly ahead of the original MPC algorithm in reaching the target path.

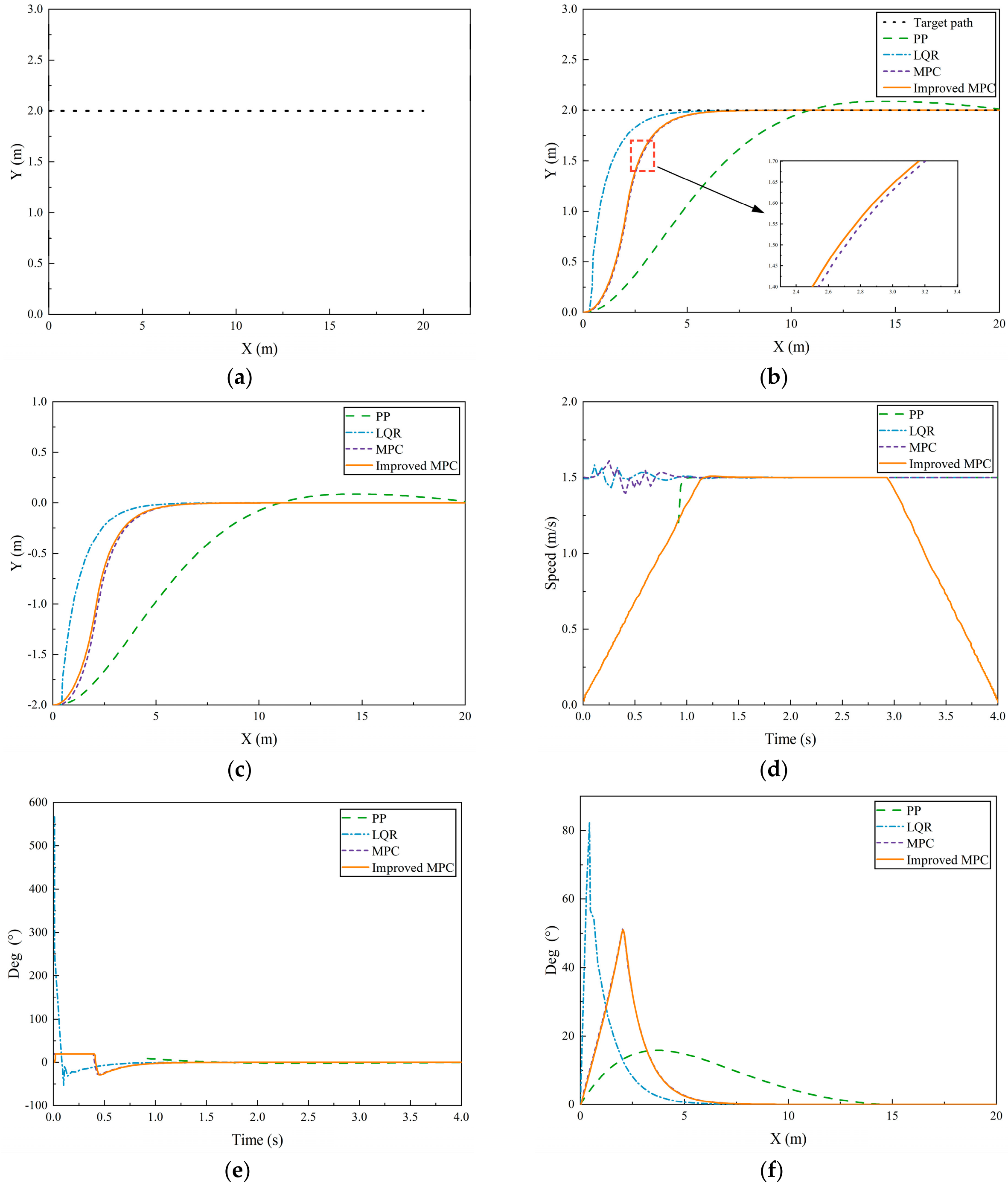

Figure 6. Trajectory and key parameters for straight-line tracking: (**a**) Target path; (**b**) Tracked path; (**c**) Lateral deviation parameters; (**d**) Speed parameters; (**e**) Front wheel angle parameters; (**f**) Heading angle parameters.

Figure 6 illustrates the performance of key parameters in path tracking. Since the tracked path was straight, the lateral deviation of the algorithms aligned with the trend of the tracking path. Regarding the speed curves in Figure 6d, there was a significant speed fluctuation in the pure tracking algorithm due to the extended preview distance. While the LQR algorithm exhibited lower lateral deviation compared to other algorithms, it also caused significant sudden changes in both the front wheel angle and heading angle. These abrupt adjustments, although effective in quickly aligning with the reference path, are less suitable for real-world motion conditions, particularly in heavy-duty AGV applications where smooth transitions are essential to maintaining stability. In contrast, the improved MPC algorithm demonstrated a more balanced approach by ensuring smoother speed transitions and more stable path tracking. This makes it more suitable for heavy-duty forklift AGV operations, where both precision and stability are critical. The improved MPC algorithm detected a curvature of 0 in the reference path, thus executing path tracking actions for straight-line segments. As depicted in Figure 6, the heading angle and steering angle variation curves of the improved MPC algorithm were almost identical to those of the MPC algorithm. With constant acceleration as the control variable, the speed curve changed smoothly without sudden fluctuations. It is worth noting that the path here was only for testing the performance of the improved algorithm; in actual warehouse operations, the initial deviation from the reference path is minimal.

The data for the maximum, minimum, average, standard deviation, and evaluation values of four algorithms (PP, LQR, MPC, improved MPC) in tracking the lateral deviation of straight-line segments are shown in Table 5. The average lateral deviation of the pure tracking algorithm was higher than those of the other algorithms, and its standard deviation was also the highest, resulting in significantly elevated evaluation values compared to the other algorithms. The evaluation value of the LQR algorithm was the lowest, but the significant sudden changes in front wheel angle and heading angle did not align with real-world motion conditions (Figure 6). The lateral deviation value of the improved MPC algorithm was higher than that of the MPC algorithm. However, as shown in Figure 6, its lateral deviation curve was better than that of the MPC algorithm. This was because the improved MPC algorithm included acceleration and deceleration phases. The significant difference between the velocity and the rated velocity led to shorter path tracking distances during simulation, thereby generating more tracking points. In cases of initial large deviation, more tracking data points amplified the lateral deviation of the system, resulting in a curve that appeared better but with poorer computational values.

Table 5. Lateral deviation data for line segments.

Algorithm	max(e_y)/m	min(e_y)/m	avg(e_y)/m	σ(e_y)/m	Ce
PP	2	1.16×10^{-3}	0.556	0.676	30.253
LQR	2	6.10×10^{-9}	0.203	0.506	12.050
MPC	2	1.79×10^{-8}	0.255	0.560	14.820
Improved MPC	2	1.83×10^{-8}	0.589	0.836	32.365

3.3.2. The Turning Condition

The turning motion is another key movement for the heavy-duty forklift-style AGV. A right-turn reference path was designed, as depicted in Figure 7a. This path formed a semicircle with a center coordinate of (0, 10) and a radius of 10 m. The starting coordinates of the AGV were (0, 2), with an initial heading angle of π and an initial velocity of 0.1 m/s.

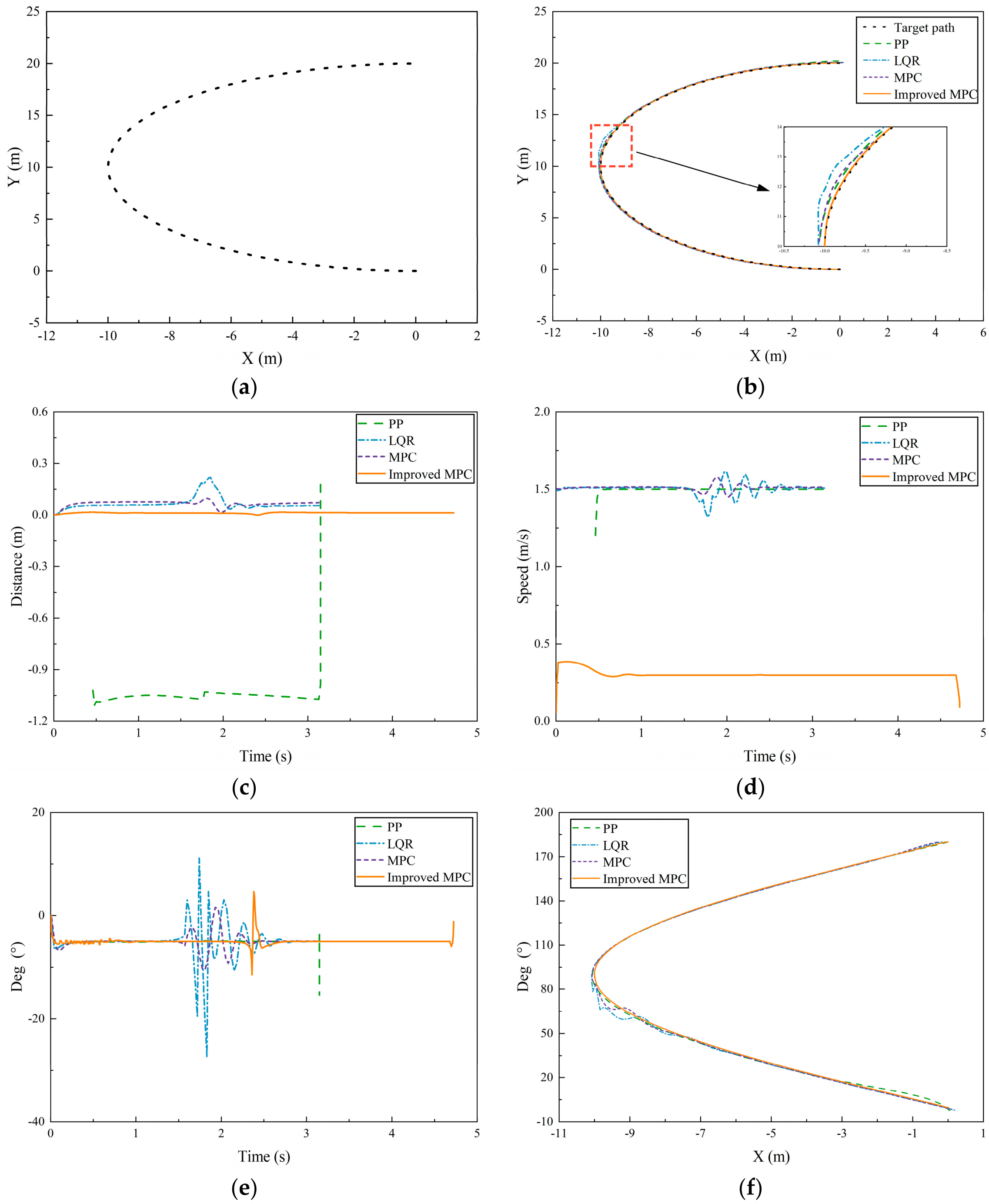

Figure 7. Trajectory and key parameters for right turns: (**a**) Target path; (**b**) Tracked path; (**c**) Lateral deviation parameters; (**d**) Speed parameters; (**e**) Front wheel angle parameters; (**f**) Heading angle parameters.

The tracked paths for the steering condition are shown in Figure 7b. Initially, there was minimal deviation among the tracking paths of the various algorithms, but as they moved toward the midpoint, the differences increased. Zooming in on the curve at this midpoint revealed that the tracking curve of the improved MPC algorithm closely aligned with the reference curve, followed by the pure tracking algorithm, the MPC algorithm, and the LQR algorithm, respectively. This consistency with the lateral deviation curves of the four algorithms in Figure 7 indicated that the improved MPC algorithm had the smallest lateral deviation, significantly differing from the other algorithms.

The pure tracking algorithm exhibited relatively smooth changes in front wheel angle and heading angle at the midpoint, but there was some fluctuation in the heading angle at the initial and endpoint positions (Figure 7). Both the LQR and MPC algorithms exhibited more pronounced changes in front wheel angle at the midpoint, resulting in larger lateral deviations at that position. The front wheel angle of the improved MPC algorithm exhibited slight fluctuations at the initial position but quickly corrected itself, with the shortest duration of fluctuations at the midpoint and a rapid return to 0 at the endpoint. The speed change trends of the LQR and MPC algorithms were similar, but the MPC algorithm's speed oscillation duration was shorter. During the acceleration phase of the improved MPC algorithm, the maximum speed slightly exceeded the rated speed. Subsequently, after feedback adjustment, the speed gradually decreased to the rated speed, with a smooth reduction to nearly 0 m/s near the endpoint.

Table 6 presents the lateral deviation data for the simulation of right-turn conditions before and after algorithm improvement. While the pure tracking algorithm showed a smaller standard deviation of lateral deviation, it exhibited the largest average deviation and evaluation value, indicating that the pure tracking controller struggled to effectively track the lookahead point with a larger preview distance. The average lateral deviation of the LQR and MPC algorithms did not differ significantly, but the superior stability of the MPC algorithm was evident from the maximum lateral deviation and standard deviation.

Table 6. Lateral deviation data for right steering.

Algorithm	max(e_y)/m	min(e_y)/m	avg(e_y)/m	σ(e_y)/m	Ce
PP	1.107	0.983	1.055	0.016	53.009
LQR	0.220	9.19×10^{-18}	0.066	0.041	3.490
MPC	0.098	9.19×10^{-18}	0.066	0.017	3.384
Improved MPC	0.016	0	0.012	0.003	0.593

The evaluation indicators for lateral deviation of the improved MPC algorithm were significantly smaller than those of the original MPC algorithm, demonstrating a notable improvement in path tracking performance. Compared to the pure tracking algorithm, LQR algorithm, and original MPC algorithm, the average lateral deviation of the improved algorithm decreased by 98.9%, 82.5%, and 82.5%, respectively. Overall, the improved MPC algorithm demonstrated the smoothest speed changes, minimal lateral deviation, and excellent control sensitivity over curve segments.

3.3.3. Double Lane Change Condition

"Double lane change" was selected to validate the performance of the improved algorithm in complex conditions of path tracking. The expression for the double lane change was defined by the following equations [23]:

$$Y_{ref}(X) = \frac{d_{y1}}{2}[1 + \tanh(z_1)] - \frac{d_{y2}}{2}[1 + \tanh(z_2)] \tag{10}$$

$$\varphi_{ref}(X) = \arctan\left[d_{y1}\left(\frac{1}{\cosh(z_1)}\right)^2\left(\frac{1.2}{d_{x1}}\right) - d_{y2}\left(\frac{1}{\cosh(z_2)}\right)^2\left(\frac{1.2}{d_{x2}}\right)\right] \tag{11}$$

where $z_1 = 2.4\,(X - 27.19)/25 - 1.2$, $z_2 = 2.4\,(X - 56.46)/21.95 - 1.2$, $d_{x1} = 25$, $d_{x2} = 21.95$, $d_{y1} = 4.05$, and $d_{y2} = 5.7$.

Figure 8a shows the double lane change reference path, which includes both straight and curved segments. Different path tracking algorithms were simulated under the double lane change condition. All algorithms performed well on straight segments, but errors were more pronounced on curved parts. Zooming in on the paths at a lateral distance of 50 m revealed that the path generated by the pure tracking algorithm lay below the reference path, followed by the original MPC algorithm and the LQR algorithm. The path tracked by the improved MPC algorithm almost perfectly aligned with the reference path, indicating superior tracking performance, especially in regions with high curvature.

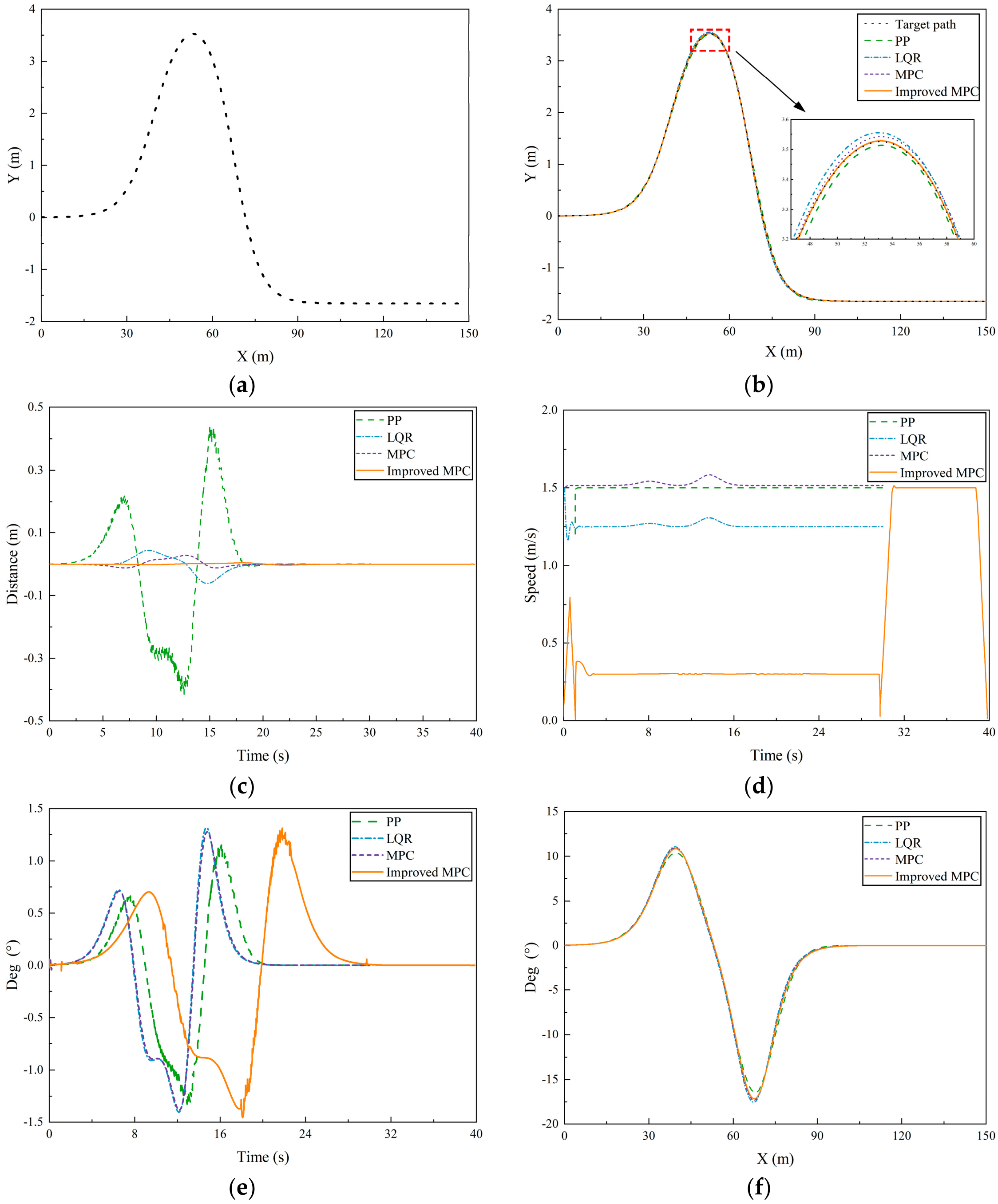

Figure 8. Trajectory and key parameters for double lane change: (**a**) Target path; (**b**) Tracked path; (**c**) Lateral deviation parameters; (**d**) Speed parameters; (**e**) Front wheel angle parameters; (**f**) Heading angle parameters.

Although the pure tracking algorithm maintained relatively stable operation at the target speed, it showed a small front wheel angle and large heading angle deviation at the two positions with maximum curvature, resulting in the highest lateral deviation. The highest speed of the LQR algorithm fluctuated around 1 m/s, making it difficult to reach the rated speed, and it also exhibited a relatively large lateral deviation.

The speed of the MPC algorithm was consistently slightly higher than 1.5 m/s, while there was noticeable fluctuation at positions with high curvature. The control quantities of the heading angle and front wheel angle were similar to those of the LQR algorithm, with a slightly smaller lateral deviation.

The improved MPC algorithm maintained relatively smooth speed changes on both straight and curved segments. Due to the short straight segment at the initial pose, the algorithm did not reach 1.5 m/s before beginning to decelerate. On curved segments, the speed initially accelerated to slightly above 0.3 m/s before decreasing to the rated speed, with almost no fluctuation in speed at positions with high curvature. When transitioning to the straight segment near the endpoint, the improved MPC algorithm had a longer distance for acceleration and deceleration, enabling it to smoothly reach the maximum speed of 1.5 m/s.

The improved MPC algorithm effectively divided the double lane change reference path into three independent segments. In straight-line and turning conditions, the improved MPC algorithm exhibited a minor adjustment in the front wheel angle at the beginning of tracking each segment, which quickly corrected itself. This phenomenon occurred for a very short duration, consistent with the minor abrupt changes in the front wheel angle variation curve observed in the double lane change simulation results.

The evaluation values of the four algorithms under the double lane change condition are shown in Table 7. The values in each column decreased gradually from top to bottom, indicating a reduction in lateral deviation and an improvement in controller tracking performance. Compared to the pure tracking algorithm, the LQR algorithm, and the original MPC algorithm, the improved algorithm reduced the average lateral deviation by 99%, 91.4%, and 82.4%, respectively.

Table 7. Lateral deviation data for double lane change.

Algorithm	$max(e_y)$/m	$min(e_y)$/m	$avg(e_y)$/m	$\sigma(e_y)$/m	Ce
PP	0.436	3.143×10^{-9}	0.097	0.129	5.325
LQR	0.061	0	0.011	0.017	0.625
MPC	0.029	0	0.005	0.008	0.303
Improved MPC	0.008	0	0.00	0.002	0.086

3.3.4. Field Experiment of Path Tracking

The experimental path for the heavy-duty forklift AGV included straight sections, curved turns, and loading/unloading paths. Figure 9 shows the actual movement paths obtained from five experiments. In the experimental scenario, obstacles restricted the movement channels, leading to a slight inclination in the planned straight sections to prevent collisions. The heavy-duty forklift AGV started from the bottom right corner of the path shown in Figure 9, first traveling along a long straight section. It then performed a turning maneuver at the curved section in the top right corner. Next, it moved from right to left along a shorter straight segment toward the target location, where it executed the loading/unloading operation at the top left corner.

The vertical path in the top left corner of Figure 9 represents the loading/unloading route. Upon reaching the loading point in the top left corner, the heavy-duty forklift AGV followed this path. During the loading/unloading process, the AGV rotated around the symmetric center of its two auxiliary wheels, aligning the forks with the pallet slots, and then reversed into the pallet position. Ideally, the path tracking point, which was the center of rotation, should have remained fixed. However, due to factors such as ground friction, the actual rotation center slightly shifted, causing minor deviations in the tracking path. This could be observed in the enlarged inset of Figure 9.

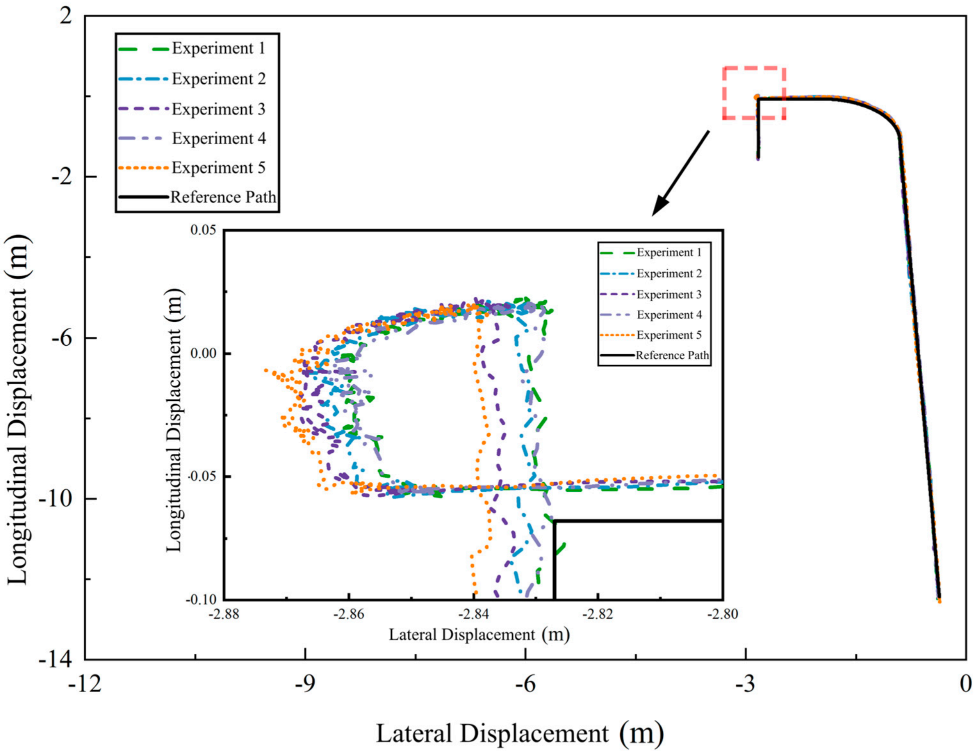

Figure 9. The experimental displacement path for the entire process.

Table 8 presents the lateral deviation data from the entire path tracking experiment. The average standard deviation of the lateral deviation was 0.017 m, while the average maximum, minimum, and mean lateral deviations were 0.065 m, 0 m, and 0.021 m, respectively. The larger lateral deviations observed during the loading/unloading path due to the spinning motion resulted in higher overall maximum, mean, and standard deviation values for the lateral deviation. However, since the reference path was nearly centered within the rack aisles and the AGV's geometric dimensions were accounted for in the path planning, there was no collision between the AGV and the racks, even at the maximum lateral deviation.

Table 8. Tracking deviations throughout the entire path.

Experiment Number	$\max(e_y)$/m	$\min(e_y)$/m	$\mathrm{avg}(e_y)$/m	$\sigma(e_y)$/m
1	0.066	0	0.019	0.016
2	0.065	0	0.021	0.016
3	0.065	0	0.023	0.017
4	0.065	0	0.019	0.016
5	0.065	0	0.023	0.017

The speed profile for the entire process is shown in Figure 10. From approximately 0 to 15 s, the AGV's speed varied along the longer straight section. Due to the insufficient path length, the AGV began to decelerate before reaching its maximum speed. The period from 15 to 22 s represented the turning phase, during which the vehicle accelerated to around 0.3 m/s to navigate the curve. The shorter straight segment lasted from about 22 to 25 s, where the path's brevity limited the AGV's ability to accelerate to its maximum speed. From 25 to 44 s, the AGV performed the spinning motion for loading/unloading, with the tracking center being the rotation center, resulting in an almost zero speed during this phase. The reverse driving phase for loading/unloading occurred from 44 to 52 s, during which the AGV moved at a low speed to insert the forks into the pallet. Subsequent control of the fork and mast enabled the completion of the loading/unloading process. Throughout the entire process, the path tracking control algorithm maintained effective tracking performance with minimal lateral deviation and stable speed control.

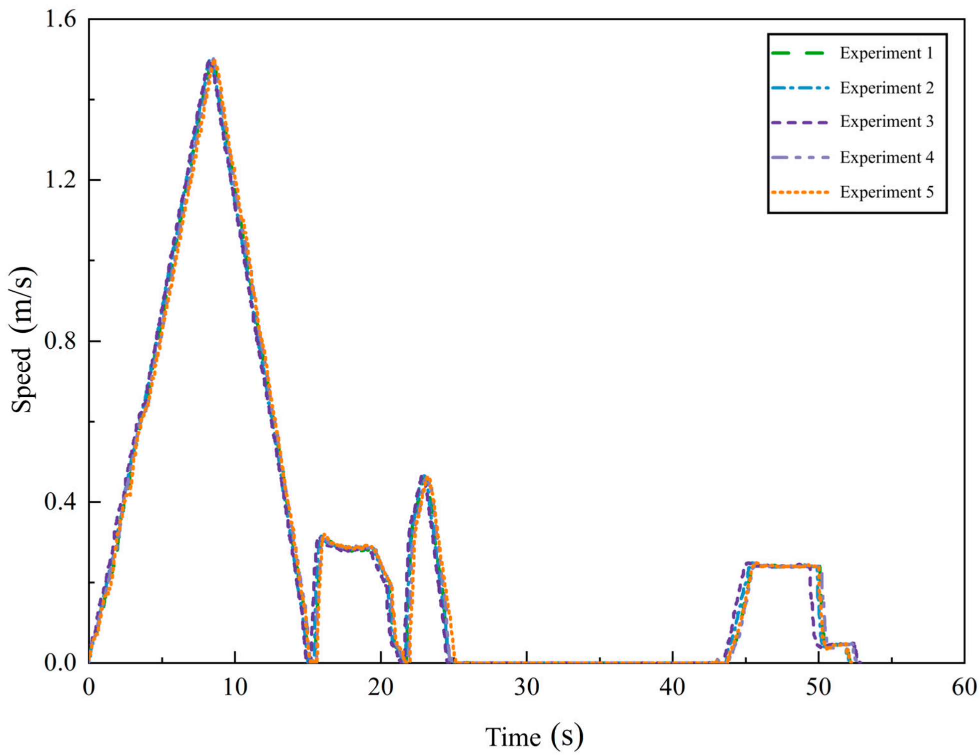

Figure 10. The experimental speed curve of the entire process.

4. Discussion

The simulation results under both normal and complex conditions indicated that the proposed velocity-adaptive MPC algorithm exhibited minimal lateral deviation, facilitating efficient navigation through narrow passages. The improved algorithm ensures smooth speed control, resulting in higher vehicle stability during material handling. Overall, its performance surpasses that of the original MPC, LQR, and pure tracking algorithms.

Compared to the simulation results, the lateral deviation values in the real vehicle experiments increased significantly. Additionally, the fluctuations in the movement speed were more pronounced. This was due to the forces acting on the vehicle in the actual handling environment, which noticeably affected the control precision. The tracking algorithm based solely on the kinematic model could not achieve low lateral deviation, and the tracking process was constrained by the real vehicle's hardware and software performance. However, since the algorithm expanded the obstacle boundaries during path planning, the actual path remained within the safety threshold, preventing collisions between the heavy-duty forklift AGV and the walls or racks. Therefore, the proposed velocity-adaptive MPC-based path tracking method can be effectively applied in narrow aisle warehouse environments.

In the context of path tracking for heavy-duty AGVs, it is crucial to consider robust control criteria to ensure system stability and performance under various uncertainties and disturbances. One such robust control approach is H-infinity control, which is designed to handle model uncertainties and external disturbances effectively. While the proposed VA-MPC method demonstrated promising results, incorporating H-infinity control criteria could further enhance its robustness. This would be particularly beneficial in scenarios where the AGV operates under varying load conditions or encounters unexpected environmental changes.

Moreover, a significant practical challenge in implementing MPC for path tracking is the requirement for full-state knowledge. In real-world applications, it is often challenging to obtain accurate measurements of all necessary states, such as sideslip angle, especially with low-cost sensors. As noted in recent studies, the accurate estimation of sideslip angle is critical for maintaining vehicle stability and ensuring safe operation, particularly in scenarios involving high-speed maneuvers or low-adhesion surfaces [24,25].

For vehicles with a high center of gravity, the roll angle becomes a crucial factor in preventing rollover incidents during path tracking. The control system must account for this by incorporating mechanisms to mitigate the risk of rollover, which is particularly important when the vehicle is executing sharp turns or operating on uneven terrain. Recent advancements in control strategies, such as the use of polytopic linear parameter-varying (LPV) control approaches, have shown promise in addressing these challenges by considering vehicle roll dynamics and employing active suspension systems to enhance both safety and comfort [24].

By integrating these robust control criteria and addressing the practical challenges associated with full-state knowledge and vehicle dynamics, the proposed VA-MPC algorithm could be further improved to ensure safe and efficient operation in a wider range of scenarios, including those with significant environmental and operational uncertainties. Future work could explore the integration of event-triggered control schemes and IoT-based solutions to improve state estimation accuracy and reduce the computational burden on the control system [25].

5. Conclusions

This work demonstrated the feasibility of a velocity-adaptive MPC-based path tracking method for heavy-duty forklift AGVs. The proposed approach is composed of several stages. First, the motion characteristics of the heavy-duty forklift AGV were analyzed. Its motion was categorized into straight-line and curve-turning motions, with the reference path divided into corresponding straight and curved sections based on curvature. Subsequently, the optimal sampling times, prediction horizon, and control horizon for low-speed driving were determined through simulation analysis. Finally, the performance of the proposed algorithm was evaluated and compared in terms of tracking accuracy and stability under various conditions, including straight-line, turning, and complex double lane change scenarios. Simulation results indicated that the VA-MPC algorithm significantly reduced lateral deviation compared to traditional methods. Specifically, under complex double lane change conditions, the improved MPC algorithm reduced the average lateral deviation by 99%, 91.4%, and 82.4% compared to the pure tracking algorithm, the LQR algorithm, and the original MPC algorithm, respectively. In addition, the field experiments carried out with the heavy-duty forklift AGV in a warehouse environment validated the feasibility and effectiveness of the proposed path tracking method. Overall, the VA-MPC algorithm ensures smooth speed transitions and higher stability during start-up and stopping phases, enhancing the safety and efficiency of heavy-duty material handling in narrow warehouse passages.

Author Contributions: Conceptualization, Y.W. and W.Z.; methodology, K.S. and X.J.; validation, Y.W., K.S., and W.Z.; formal analysis, Y.W. and K.S.; resources, X.J.; data curation, W.Z.; writing—original draft preparation, Y.W.; writing—review and editing, W.Z. and X.J. All authors have read and agreed to the published version of the manuscript.

Funding: This research received funding from the scientific and technological innovation project (Project No.: E210100326) from State Energy Group Shendong Coal Group Co., Ltd.

Data Availability Statement: Data are contained within the article.

Conflicts of Interest: Author Yajun Wang was employed by the company State Energy Group Shendong Coal Group Co., Ltd. Authors Kezheng Sun and Xiaojun Jin were employed by the company Zhongcang Robot (Nan Jing) Co., Ltd. The remaining authors declare that the research was conducted in the absence of any commercial or financial relationships that could be construed as a

potential conflict of interest. The authors declare that this study received funding from State Energy Group Shendong Coal Group Co., Ltd. The funder was not involved in the study design, collection, analysis, interpretation of data, the writing of this article or the decision to submit it for publication.

Abbreviations

AGV	Automated Guided Vehicle
PP	Pure Pursuit
MPC	Predictive Control Model
VA-MPC	Velocity-Adaptive MPC
LQR	Linear Quadratic Regulator
ROS	Robot Operating System
Nomenclature	
φ	The heading angle
v	The velocity of the vehicle
a	The acceleration of the vehicle
δ	The steering angle
r	The reference point in the reference path
$\widetilde{\chi}(k)$	The changes in the error of the state variables
$\widetilde{\boldsymbol{u}}(k)$	The changes in the error of the control variables
$\widetilde{A}$	The state matrix
$\widetilde{B}$	The control matrix
N_{P}	The prediction horizon
N_{C}	The control horizon
Υ	The prediction error vector
Ψ	The system state transition matrix
ΔU	The control increment vector
Θ	The system response matrix

References

1. Anane, M.A.; Bagheri, F.; Cepolina, E.M.; Tonelli, F. Impact of Transportation Costs on the Establishment of an Industrial Symbiosis Network. *Sustainability* **2023**, *15*, 19. [CrossRef]
2. Cheng, W.L.; Meng, W.J. An efficient genetic algorithm for multi AGV scheduling problem about intelligent warehouse. *Robot. Intell. Autom.* **2023**, *43*, 382–393. [CrossRef]
3. Liu, J.C.; Jayakumar, P.; Stein, J.L.; Ersal, T. A nonlinear model predictive control formulation for obstacle avoidance in high-speed autonomous ground vehicles in unstructured environments. *Veh. Syst. Dyn.* **2018**, *56*, 853–882. [CrossRef]
4. Bányai, T. Energy Efficiency of AGV-Drone Joint In-Plant Supply of Production Lines. *Energies* **2023**, *16*, 28. [CrossRef]
5. Yu, C.W.; Liao, W.Z.; Zu, L.T. Dynamic Scheduling Optimization Method for Multi-AGV-Based Intelligent Warehouse Considering Bidirectional Channel. *Systems* **2024**, *12*, 24. [CrossRef]
6. Li, J.X.; Cheng, W.J.; Lai, K.K.; Ram, B. Multi-AGV Flexible Manufacturing Cell Scheduling Considering Charging. *Mathematics* **2022**, *10*, 15. [CrossRef]
7. Badgujar, C.; Das, S.; Figueroa, D.M.; Flippo, D.; Welch, S. Deep neural networks to predict autonomous ground vehicle behavior on sloping terrain field. *J. Field Robot.* **2023**, *40*, 919–933. [CrossRef]
8. Chiu, M.C.; Yeh, L.J.; Lai, G.J.; Huang, B.M. Developing an auto-tracking automated guided vehicle carrier using a wave-varied detecting method. *Proc. Inst. Mech. Eng. Part C-J. Eng. Mech. Eng. Sci.* **2010**, *224*, 1349–1357. [CrossRef]
9. Stefanini, R.; Vignali, G. Environmental and economic sustainability assessment of an industry 4.0 application: The AGV implementation in a food industry. *Int. J. Adv. Manuf. Technol.* **2022**, *120*, 2937–2959. [CrossRef]
10. Saiz-Rubio, V.; Rovira-Más, F.; Cuenca-Cuenca, A.; Alves, F. Robotics-based vineyard water potential monitoring at high resolution. *Comput. Electron. Agric.* **2021**, *187*, 12. [CrossRef]
11. Lin, J.W.; Siao, C.Y.; Chien, T.H.; Chang, R.G. A Novel Automatic Meal Delivery System. *Intell. Autom. Soft Comput.* **2021**, *29*, 685–695. [CrossRef]
12. Mai, T.A.; Dang, T.S.; Duong, D.T.; Le, V.C.; Banerjee, S. A combined backstepping and adaptive fuzzy PID approach for trajectory tracking of autonomous mobile robots. *J. Braz. Soc. Mech. Sci. Eng.* **2021**, *43*, 13. [CrossRef]
13. Zhao, S.A.; Zhao, G.X.; He, Y.; Diao, Z.H.; He, Z.D.; Cui, Y.X.; Jiang, L.Y.; Shen, Y.P.; Cheng, C. Biomimetic Adaptive Pure Pursuit Control for Robot Path Tracking Inspired by Natural Motion Constraints. *Biomimetics* **2024**, *9*, 17. [CrossRef]
14. Choi, Y.; Lee, W.; Kim, J.; Yoo, J. A Variable-Sampling Time Model Predictive Control Algorithm for Improving Path-Tracking Performance of a Vehicle. *Sensors* **2021**, *21*, 20. [CrossRef] [PubMed]

15. Hu, M.; Wei, X.; Wang, A.; Shi, S.; Chen, S. Path Tracking Control Method of Tractor Based on Adaptive Model Prediction Control. *J. Agric. Mech. Res.* **2024**, *46*, 227–233.
16. Wang, C.C.; Liu, X.F.; Yang, X.Q.; Hu, F.; Jiang, A.M.; Yang, C.G. Trajectory Tracking of an Omni-Directional Wheeled Mobile Robot Using a Model Predictive Control Strategy. *Appl. Sci.* **2018**, *8*, 15. [CrossRef]
17. Barreno, P.; Parras, J.; Zazo, S. An Efficient Underwater Navigation Method Using MPC with Unknown Kinematics and Non-Linear Disturbances. *J. Mar. Sci. Eng.* **2023**, *11*, 20. [CrossRef]
18. Demir, A.S.; Mumcu, E. Analysis of automated guided vehicle use in health care by simulation: A case study in a university hospital. *Concurr. Comput. -Pract. Exp.* **2022**, *34*, 9. [CrossRef]
19. Gong, G.Y.; Gan, C.Q.; Fang, Y.; Zhu, Y.F.; Hu, Q.Y. Link-Blockage Model and AP-Placement Scheme for No-Blockage Link between AGV and AP in Logistics-Warehousing VLC Network. *Photonics* **2023**, *10*, 17. [CrossRef]
20. Li, Y.; Wang, D.; Feng, Q.; Liu, Y.; Nan, Y. Contrastive Study on Path Tracking Control Methods for Commercial Vehicles. In Proceedings of the China SAE Congress 2020, Shanghai, China, 27–29 October 2020; Springer: Singapore, 2022.
21. Ye, B.; Niu, S.; Li, L.; Wu, W. A Comparison Study of Kinematic and Dynamic Models for Trajectory Tracking of Autonomous Vehicles Using Model Predictive Control. *Int. J. Control. Autom. Syst.* **2023**, *21*, 3006–3021. [CrossRef]
22. Kanchwala, H.; Viana, I.B.; Aouf, N. Cooperative path-planning and tracking controller evaluation using vehicle models of varying complexities. *Proc. Inst. Mech. Eng. Part C-J. Eng. Mech. Eng. Sci.* **2021**, *235*, 2877–2896. [CrossRef]
23. Wang, S.P.; Wang, Z.Y.; Jiang, R.; Zhu, F.; Yan, R.D.; Shang, Y. A multi-agent reinforcement learning-based longitudinal and lateral control of CAVs to improve traffic efficiency in a mandatory lane change scenario. *Transp. Res. Pt. C-Emerg. Technol.* **2024**, *158*, 18. [CrossRef]
24. Viadero-Monasterio, F.; Nguyen, A.-T.; Lauber, J.; Boada, M.J.L.; Boada, B.L. Event-triggered robust path tracking control considering roll stability under network-induced delays for autonomous vehicles. *IEEE Trans. Intell. Transp. Syst.* **2023**, *24*, 14743–14756. [CrossRef]
25. Viadero-Monasterio, F.; García, J.; Meléndez-Useros, M.; Jiménez-Salas, M.; Boada, B.L.; López Boada, M.J. Simultaneous Estimation of Vehicle Sideslip and Roll Angles Using an Event-Triggered-Based IoT Architecture. *Machines* **2024**, *12*, 53. [CrossRef]